

Biofouling

The Journal of Bioadhesion and Biofilm Research

ISSN: 0892-7014 (Print) 1029-2454 (Online) Journal homepage: <http://www.tandfonline.com/loi/gbif20>


Biofouling in membrane bioreactors: nexus between polyacrylonitrile surface charge and community composition

Lisendra Marbelia, Marie-Aline Hernalsteens, Shazia Ilyas, Basak Öztürk, Anthony Szymczyk, Dirk Springael & Ivo Vankelecom

To cite this article: Lisendra Marbelia, Marie-Aline Hernalsteens, Shazia Ilyas, Basak Öztürk, Anthony Szymczyk, Dirk Springael & Ivo Vankelecom (2018): Biofouling in membrane bioreactors: nexus between polyacrylonitrile surface charge and community composition, *Biofouling*, DOI: [10.1080/08927014.2018.1428311](https://doi.org/10.1080/08927014.2018.1428311)

To link to this article: <https://doi.org/10.1080/08927014.2018.1428311>

 View supplementary material 

 Published online: 15 Feb 2018.

 Submit your article to this journal 

 View related articles 

 View Crossmark data 



Biofouling in membrane bioreactors: nexus between polyacrylonitrile surface charge and community composition

Lisendra Marbelia^a, Marie-Aline Hernalsteens^a, Shazia Ilyas^{a,d}, Basak Öztürk^b, Anthony Szymczyk^c, Dirk Springael^b and Ivo Vankelecom^a

^aCentre for Surface Chemistry and Catalysis, Faculty of Bioscience Engineering, KU Leuven, Leuven, Belgium; ^bLaboratory of Soil and Water Management, Faculty of Bioscience Engineering, KU Leuven, Leuven, Belgium; ^cISCR (Institut des Sciences Chimiques de Rennes), Univ Rennes, CNRS, Rennes, France; ^dUrban Sector Planning & Management Services Unit. (Pvt.) Ltd. (The Urban Unit), Lahore, Pakistan.

ABSTRACT

The influence of membrane surface charge on biofouling community composition during activated sludge filtration in a membrane bioreactor was investigated in this study using polyacrylonitrile-based membranes. Membranes with different surface properties were synthesized by phase inversion followed by a layer-by-layer modification. Various characterization results showed that the membranes differed only in their surface chemical composition and charge, ie two of them were negative, one neutral and one positive. Membrane fouling experiments were performed for 40 days and the biofouling communities were analyzed. PCR-DGGE fingerprinting indicated selective enrichment of bacterial populations from the sludge suspension within the biofilms at any time point. The biofilm community composition seemed to change with time. However, no difference was observed between the biofilm community of differently charged membranes at specific time points. It could be concluded that membrane charges do not play a decisive role in the long-term selection of the key bacterial foulants.

ARTICLE HISTORY

Received 6 October 2017
Accepted 8 January 2018

KEYWORDS

Membrane bioreactor; polyacrylonitrile; surface charge; layer-by-layer; biofouling; PCR-DGGE fingerprinting

Introduction

The quantity and size of membrane bioreactors (MBRs) worldwide has increased exponentially with capacities ranging from $< 1 \text{ m}^3 \text{ day}^{-1}$ to $> 100,000 \text{ m}^3 \text{ day}^{-1}$ (Zhang, Chua, et al. 2006). However, aside from the high investment cost, one of the main drawbacks and research challenges of membrane technology remains membrane fouling. Biofouling refers to fouling resulting from the undesirable gradual attachment on the wet membrane surface of individual cells, cell clusters or materials of biological origin present in the mixed liquor (Vanysacker et al. 2014). Researchers have extensively discussed five either sequential or simultaneous steps in the formation of a three-dimensional biofilm (Stoodley et al. 2002; Vanysacker et al. 2014): formation of a conditioning film, reversible and irreversible bacterial attachment, production of extracellular polymeric substances, micro-colony formation and biofilm maturation, and bacterial detachment.

There are three main interdependent parameters having an influence on membrane fouling and sludge filterability (Zhang, Chua, et al. 2006): the nature of the hydrodynamic

environment, the properties of the membrane, and the characteristics of the sludge (i.e. the biopolymer concentration and the microbial community structure), which in turn are affected by operating parameters impacting on biomass growth and decay. In general, membrane design involves the adjustment of the membrane properties so as to reduce the affinity of the solutes with the membrane surface (Field et al. 1995).

Generally, it is known that hydrophilic smooth membranes with high porosity and narrow pore size distribution tend to have less fouling (Le-Clech et al. 2006). Solutes and bacteria in the mixed liquor tend to show a greater affinity towards hydrophobic membranes. Thus, it leads to more severe fouling than on hydrophilic membranes (Pasmore et al. 2001; Meng et al. 2009; Le-Clech 2010), where the bacteria-membrane interactions are more reversible (Pasmore et al. 2001). Although research is being performed in order to increase the hydrophilicity of hydrophobic membranes (Mansouri et al. 2010; Kochkodan and Hilal 2015), it has been reported that the degree of hydrophilicity of a membrane is not a good indicator of biofouling tendency (Liu et al. 2010).

For the surface charge, electrostatic repulsion between the particles and the membrane surface will occur if they bear the same charge, thus reducing fouling tendency by electrostatic repulsion forces between them (Kochkodan and Hilal 2015). However, Pasmore et al. (2001) found that biofouling initiation (tested for two days) is minimized when membranes are electrically neutral and increases with increasing positive or negative charge. This is most surprising since particles and bacteria must overcome the electrical double layer formed in electrolytes and adjacent to the charged membrane surface as well as around their own cell membrane in order to attach to the surface (Schaep and Vandecasteele 2001). Most bacteria carry a net negative surface charge in aqueous environments due to the presence of phospholipids, (lipo)polysaccharides and proteins in their cell membrane (Jucker et al. 1996; Pasmore et al. 2001). Thus, it is expected that negatively charged membrane surfaces will impede bacterial attachment. However, Gottenbos et al. (2001) reported that although negatively charged surfaces reduce the chance of initial bacterial adhesion and thus delay the formation of a biofilm, the initially attached Gram-negative bacteria did not develop further on positively charged surfaces. This is due to strong electrostatic attractions that impede bacterial elongation and division (Roosjen et al. 2006). Conversely, Gram-negative as well as Gram-positive bacteria did grow exponentially on negatively charged surfaces after initial adhesion (Gottenbos et al. 2001).

For low-fouling and anti-adhesion strategies, different synthesis/modification approaches are applied. Polymer blending, grafting and coating are known methods to prepare membranes with improved surface properties (ie hydrophilicity and different surface charge) (Mansouri et al. 2010; Kochkodan and Hilal 2015). For membranes with a different surface charge, the electrical properties of their surfaces can be modified by coating with different polycations or polyanions, eg by using the layer-by-layer (LbL) technique (Joseph et al. 2014).

The purpose of this study was to elucidate the relationship between the specific surface charge (neutral, positive, negative) of polyacrylonitrile (PAN) membranes prepared by phase inversion but then further modified *via* wet chemistry approaches, and the development and composition of the microbial community in the biofouling layer developed during 40 days in a submerged laboratory-scale aerobic membrane bioreactor operated on synthetic feed.

The effect of membrane composition on biofilm community structure and diversity is assessed by answering three questions: (1) does the bacterial biofouling community differ from the sludge community at a certain time point, ie are bacterial populations from the sludge specifically enriched within a biofilm? (2) does the bacterial biofouling community change with time, ie do temporal

variations in local conditions favor or exclude specific bacterial populations? and (3) does the bacterial biofouling community on a membrane differ from one membrane to another type at a certain time point, ie do the membrane surface charges affect the composition of the biofilm community?

Materials and methods

Membrane and module preparation

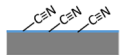
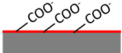
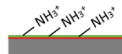
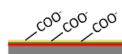
The PAN flat-sheet membranes were prepared *via* phase-inversion (Hořda and Vankelecom 2015) from a well-mixed 11 and 13wt% PAN (Average MW 150,000 g mol⁻¹, Scientific Polymer Products, New York, USA) in dimethyl sulfoxide (DMSO, Acros Organics, Geel, Belgium). The bubble-free polymer solution was cast on a polyethylene/polypropylene non-woven support (Novatex 2471, Freudenberg, Germany) at a casting speed of 2.25 cm s⁻¹ to form 250 μm wet thickness films. The cast films were then directly immersed in the non-solvent bath (demineralized H₂O).

The choice of 11 and 13 wt% PAN solutions to prepare the different membranes is based on the requirement to finally obtain neutral membranes and charged membranes for which the fouling behavior is solely determined by charge difference and not by differences in pore size (distribution), clean water permeability or surface roughness. As the hydrolysis procedure impacted on those properties, another composition of the casting solution was required for the uncharged membrane.

Table 1 lists the types and codes of membranes which were prepared in this study. PAN (neutral) membranes were made from the 13% PAN solution. For the 11% PAN, negative charges were introduced by hydrolysis, based on the procedure described by Li et al. (2008). The membranes were immersed for 40 min at 50°C in a stirred solution containing 10 wt% NaOH (Fisher Chemical, Pittsburgh, PA, USA). This membrane was then coded as PAN-H (-). Later on, the positive charge and the second layer of the negative charge were added by dipcoating the membrane in aqueous solutions of weak polyelectrolytes by means of manual LbL deposition (Joseph et al. 2014; Ilyas et al. 2016), to prepare membrane PAN-H^{PAH} (+) and PAN-H^{PAA} (-).

For membrane PAN-H^{PAH} (+), the hydrolyzed membranes were first immersed in a rinsing solution containing 0.05 M NaNO₃ (Chem-Lab NV, Zedelgem, Belgium) in ultrapure-H₂O (pH 6) for 10 min, in order to wash the pores before the polymer layer deposition. The wash step was followed by 30 min of dipping in an aqueous solution of the polycation poly(allylamine hydrochloride) (PAH, MW 15,000 g mol⁻¹, Sigma Aldrich, Belgium) (pKa = 8–9; Choi and Rubner 2005) with a concentration of 0.1 g in

Table 1. List of the membranes prepared in this study.

Membrane type	Polymer solution	Surface modification	Surface charge	Code
	13 wt% PAN ^a	/	Neutral	PAN (neutral)
	11 wt% PAN	Hydrolysis	Negative	PAN-H (-)
	11 wt% PAN	Hydrolysis + 1 deposited layer (PAH ^b)	Positive	PAN-H ^{PAH} (+)
	11 wt% PAN	Hydrolysis + 2 deposited layers (PAH and PAA ^c)	Negative	PAN-H ^{PAA} (-)

^aPolyacrylonitrile.

^bPoly(allylamine hydrochloride).

^cPoly(acrylic acid).

1 l of rinsing solution. The composite positively charged membranes thus obtained were then immersed again in the rinsing solution for 2×10 min in order to stabilize the adsorbed layer and to remove unadsorbed/loosely attached PAH, thus preventing complexation of PAH and PAA in the next step. Half of the membranes were stored in ultrapure H₂O for further use.

For membrane PAN-H^{PAA} (-), the membrane PAN-H^{PAH} (+) continued the coating train with the polyanion (PAA). After an additional 10 min immersion in the rinsing solution, these were dipped for 30 min in a solution of 0.1 g poly(acrylic acid) (PAA, MW 15,000 g mol⁻¹, Sigma Aldrich) (pKa = 5.5–6.5; Choi and Rubner 2005) in 1 l of rinsing solution. The composite negatively charged membranes (at pH > pKa) thus obtained were then immersed again in the rinsing solution for 2×10 min and finally stored in ultrapure H₂O for further use.

The flat sheet membranes obtained were potted into envelope-sized modules (Bilad et al. 2011a). Each membrane sheet was cut at the appropriate size and folded double to form an envelope surrounding two sheets of spacer (3510 Corex, Agfa, Belgium) and a permeate channel (silicone tube), meant to connect the module interior to the peristaltic pump of the reactor. Each folded membrane was fixed to a polyvinylchloride (PVC) frame by gluing the edges together using a 50/50 mixture of binder and hardener (UHU plus, Endfest 300, Germany). The glued edges were allowed to dry overnight while keeping the membranes wet. The final modules had an effective filtration area of 2×75 cm² and were stored in demineralized H₂O for further use.

MBR

Fouling experiments were conducted using a laboratory-scale high-throughput membrane bioreactor (HT-MBR) (Marbelia et al. 2016) composed of an aerated bioreactor tank with a volume of 37.8 l which contained the 4×4 replicate membrane modules immersed

in clusters of four different membrane types in 20 l of activated sludge.

The permeate was sucked through a multichannel peristaltic pump (Watson Marlow, UK) connected to the 4×4 replicate modules and at an average total constant flow rate of (25.6 ± 3.1) l day⁻¹, corresponding to ~ 6.5 l m⁻² h⁻¹ (1 m⁻² h⁻¹) per membrane, using cycles of 8 min filtration and 2 min relaxation (Piasecka et al. 2012).

The bioreactor was inoculated with aerobic activated sludge from a sedimentation tank of the local wastewater treatment plant of Leuven (Aquafin, Leuven, Belgium). The MBR was fed with a protamylase solution through a peristaltic pump (Watson Marlow, 503S, which was connected to a level controller as to keep the sludge suspension volume constant. Each week, 1.4 l of sludge suspension were withdrawn manually from the reactor to control the sludge retention time and the total solid concentration. The MBR was operated at a sludge retention time of 100 days and an average hydraulic retention time of 18.75 h. The first 72 days, stabilization period was performed with random membranes. Later on, the fouling experiment was performed with the PAN modified membranes.

Quality measurements

The total solid (TS), the mixed liquor suspended solids (MLSS), the mixed liquor volatile suspended solids (MLVSS), the sludge volume index (SVI) and pH were monitored (WTW pH-meter 330) two times a week by taking uniform sludge samples from the middle zone of the bioreactor. Measurements were performed in triplicate.

The TS was measured by drying 3 ml of activated sludge suspension in the oven (Mettler, Germany) for 2 h at 105°C to constant weight and calculating the difference between the wet and dry samples.

The MLSS was obtained by filtration of the sludge suspension through a 0.22 μm or 0.45 μm filter paper and subsequently drying the filter residue in the oven at 105°C for 2 h to constant weight. The MLSS is obtained

by calculating the difference between the wet and dry samples.

The MLVSS concentration (g l^{-1}) was measured by drying 3 ml of activated sludge in the oven (Memmert) for 2 h at 105°C to constant weight, followed by ashing the residue in the muffle oven (B 180, Nabertherm, Germany) at 550°C for 3 h. The MLVSS was then calculated as: $\text{MLVSS} = \text{MLSS} - \text{ash}$.

The SVI (ml g^{-1}) is defined as the total volume (ml) occupied by 1 g of MLSS after sedimentation for 30 min. The settled volume was measured in twofold replicates in 100 ml graduated cylinders. The SVI was calculated according to:

$$\text{SVI} = \frac{\text{average settled volume (ml l}^{-1}\text{)}}{\text{average MLSS (g l}^{-1}\text{)}} \quad (1)$$

The sludge composition and floc structure and size were analyzed microscopically (Bx51, Olympus, Tokyo, Japan) with a $10\times$ zoom magnification and by means of the objectives UPlanFI 100 $\times/1.30$ oil Ph3 $\infty/0.17$ (magnification $100\times$), UPlanFI 40 $\times/0.75$ Ph2 $\infty/0.17$ (magnification $40\times$) and UPlanFI 10 $\times/0.30$ (magnification $10\times$) every two weeks in order to assess the quality and state of the sludge biomass and the presence of microorganisms other than bacteria in view of rapid process optimization (eg organic loading, aeration).

Analysis

Membrane characterization

Physico-chemical analysis

Attenuated total reflectance Fourier transform infrared spectroscopy (ATR-FTIR) allows determination of the functional groups present at the membrane surface, by collecting an infrared spectrum in the range $4,000\text{--}370\text{ cm}^{-1}$ and assigning chemical bonds to typical vibration typologies. Two coupon replicates per membrane type were air-dried, followed by drying in a vacuum oven (Sheldon Manufacturing 1410, VWR International, Radnor, PA, USA) at 29 Hg.vac (ie 50 mbar) (Mad.Duo2, Pfeiffer Vacuum, Germany) at room temperature for 6 h prior to analysis. The IR spectra were collected by measurements at room temperature on 2–4 points per coupon replicate using a FTIR spectrometer (Alpha-P, Bruker Corporation, Germany) and the baseline corrected with optical spectroscopy software (OPUS, Bruker Corporation).

Scanning electron microscopy (SEM) allows determination of the surface structure and membrane morphology (top layer thickness, cross-section, porosity). Air-dried samples were mounted on a SEM holder and coated with a thin layer of a mixture of gold and palladium (Sputtering Device 07120/172, Balzers Union, Liechtenstein) prior to

analysis. The membrane surface structures were analyzed using a scanning electron microscope (SEM XL30 FEG, Philips, USA) and imaging software (XL30 Microscope Control, USA).

Atomic force microscopy (AFM) allows determination of the three-dimensional micro-topography of the membrane surface. Scans were performed at tapping mode using a scanning probe microscope (PicoPlus – AFM, Series 5500, Agilent Technologies Inc., Santa Clara, CA, USA). Silicon tips (Pointprobe-Plus[®] Silicon-SPM-Sensor, Nanosensors, Germany) held by a cantilever with a thickness of $(2.0 \pm 1)\ \mu\text{m}$, a resonance frequency of 6–21 kHz and a force constant of $0.02\text{--}0.77\ \text{N m}^{-1}$ were used at a tip height of 10–15 μm . The images were flattened (1st order) in order to exclude the long-wave variations related to the substratum.

Contact angle measurements were performed by placing one drop of demineralized H_2O with a volume of 2 μl at three locations per air-dried coupon replicate with a dropper at room temperature. Directly after placing the droplet on the membrane surface, a camera recorded the time-evolution of the drop, followed by on-line measurements of the contact angle by a goniometer (DSA 10-MK2, Krüss, Hamburg, Germany). These measurements were averaged out to yield the average contact angle (θ -value).

Water uptake measurements were performed to determine the volume porosity of the membranes. Two coupon replicates per membrane type were immersed in demineralized H_2O immediately after synthesis during a non-limiting number of days ($> 72\ \text{h}$) followed by oven-drying at 60°C for 24 h. The water uptake results, calculated as a water mass loss after drying, were used to determine the volume porosity.

The electrokinetic properties of the membranes were analyzed by streaming current measurements where two identical membrane coupons were placed in an adjustable-gap measuring cell (SurPASS Electrokinetic Analyzer, Anton Paar GmbH, Austria), the distance between the membrane coupons being set to $95 \pm 5\ \mu\text{m}$. An electrolyte solution (0.001 M KCl) with pH ranging from 3 to 9 was pumped through the cell. The electrokinetic behavior was analyzed under inert N_2 atmosphere (Idil Mouhoumed et al. 2014) and a pair of Ag/AgCl electrodes monitored the streaming current. Visiolab software (Anton Paar GmbH, Austria) was used for data analysis.

Permeability-related measurements

The clean water permeance (CWP, $\text{l m}^{-2}\ \text{h}^{-1}\ \text{bar}^{-1}$) of the membrane coupons was assessed at room temperature in a dead-end high-throughput mode running 16 different membranes in parallel at a constant pressure of 1.3 bar using ultrapure H_2O (Vandezande et al. 2009). The CWP of all 16 modules was assessed at room temperature by connecting the modules, mounted vertically in a container filled with ultrapure H_2O , to a multi-channel peristaltic

pump (Watson Marlow, UK) performing cross-flow filtration by sucking ultrapure H₂O out of the module.

A modified flux-stepping experiment with activated sludge was performed on the membrane modules using the flux step method, involving 20 min filtration and 10 min relaxation (Le Clech et al. 2003; van der Marel et al. 2009). The experiment was performed in the range 3.5 to 35 l m⁻² h⁻¹, with a flux step height of 3.5 l m⁻² h⁻¹. The corresponding trans membrane pressure was recorded every 5 min (DG-10-S, WIKA, Klingenberg, Germany).

J_c is defined as the maximum flux above which deviation from the linear trend occurs by calculation of $\frac{d^2 \Delta P}{dt^2}$ (Le Clech et al. 2003). Alternatively, the determination of J_c could be based on arbitrary threshold values like a threshold fouling rate of 0.1 mbar min⁻¹ (Le Clech et al. 2003) or a threshold permeance change $K > 0.9 K_0$, with K_0 the permeance during the first flux step (Ye et al. 2005). The effect of temperature on the critical flux value was minimized by correction of J_c based on following empirical formula from (Fan et al. 2006):

$$J_c^T = J_c^{20} * 1.025^{(T-20)} \quad (2)$$

where J_c^T and J_c^{20} are the critical flux values at a sludge temperature $T = 14.2^\circ\text{C}$ during the measurements and at 20°C respectively.

Biofouling (community) characterization

Sample preparation and storage

The bacterial diversity and composition were analyzed on the feed (solution and pellet), the sludge suspension and the membrane biofilm developing on the modules. The feed samples were collected in a sterile microcentrifuge tube from the outlet of the peristaltic tubes and centrifuged (Centrifuge 5424, Eppendorf, Hamburg, Germany) at room temperature for 15 min at 12,000 rcf. The pellet was resuspended in 450 μl of glucose-Tris-EDTA (GTE) buffer (25 mM Tris-Cl, 10 mM EDTA, 50 mM glucose, pH 8.31) by vortexing at intermediate speed (< 1,600 rpm). Next, a sample of the pellet at the bottom of the feed container was collected in a sterile microcentrifuge tube on day 8 of the maintenance period. An aliquot of the pellet was resuspended in 450 μl of GTE buffer by vortexing as mentioned previously.

Table 2. Sequence and annealing temperature of the forward primer GC-63F and the reverse primer 518R.

Primer	Primer sequence (5' → 3')
Forward, GC-63F	CGC CCG CCG CGC GCG GCG GGC GGG GCG GGG GCA CGG GGG GCA GGC CTA ACA CAT GCA AGT C
Reverse, 518R	ATT ACC GCG GCT GCT GG

Sludge samples of 1 ml were taken from the middle of the reactor and collected in a sterile microcentrifuge tube. The samples were centrifuged at room temperature for 15 min at 3,000 rcf. The pellet was resuspended in 450 μl of GTE buffer by vortexing as already mentioned.

Biofilm samples of each of the 4×4 replicate modules were taken from the membrane modules. Before sampling of the biofilm, each module was taken out of the bioreactor and rinsed with demineralized H₂O for 1 min to remove all loosely attached sludge material. Biofilm samples were obtained by carefully scraping of cell material from the two identical membrane surfaces of the module over the full length of the membrane with a sterile stainless steel scraper. After sampling, the modules were immersed back in the reactor. The sample was transferred and resuspended in a sterile microcentrifuge tube containing 450 μl of GTE buffer by vortexing as mentioned previously.

These four types of samples were stored at -21°C for further DNA extraction.

Culture-independent analysis of microbial communities

DNA extraction and PCR amplification of 16S rDNA fragments. Genomic DNA was extracted using the cetyltrimethylammonium bromide (CTAB)-lysozyme method (Larsen et al. 2007) with some modifications (Supplementary Appendix 1).

PCR reactions were performed in duplicate on each DNA sample in order to obtain enough DNA for the following DGGE analysis and to overcome the PCR bias. Each PCR mix (25 μl) contained 7.5 μl of PCR water (DNase and RNase free ultrapure H₂O), 0.5 μl of GelTrack Loading Dye, 12.5 μl of AccuStart II PCR Toughmix (Quanta Biosciences Inc., Beverly, MA, USA) and 1.25 μl of each primer (10 μM). To each PCR mix 10–20 ng extracted template DNA were added, originating from the four module replicates. As the purpose was to assess the difference between membrane types, and not between replicates, these were pooled before DGGE. The eubacterial primers GC-63F forward primer and 518R reverse primer (Table 2) were used to amplify a gene fragment of 496 bp from the 16S rRNA gene. Thermocycling conditions (Eppendorf Mastercycler, Hamburg, Germany) were: 95°C for 5 min, followed by 25 amplification cycles: 94°C for 30 s, 60°C for 30 s and 72°C for 1 min. Thermocycling was ended with a final extension at 72°C for 8 min.

The DNA quantity (ng μl^{-1}) of the PCR amplicons was determined by 'broad range' Qubit measurements (Qubit® 3.0 Fluorometer, Life Technologies, Invitrogen, Carlsbad, CA, USA) following the manufacturer's instructions. Five μl of the PCR products were also examined on a 1.5% agarose gel stained with GelRed against a 2 μl GeneRuler 100 bp plus DNA-ladder. Electrophoresis was

performed at 6 V cm^{-1} for 60 min (PS 3003, Gibco BRL, San Francisco, CA, USA) in $1\times$ Tris-acetic acid-EDTA (TAE) running buffer (40 mM Tris, 20 mM acetic acid, 1 mM EDTA, pH 8.3). After electrophoresis, the gel was visualized (GeneSnap, Syngene, India) on an UV transilluminator (Bio Imaging, Syngene, India).

Denaturing gradient gel electrophoresis fingerprinting. The DGGE experiment was conducted as follows. Approximately 300 ng of PCR product of each sample were loaded on an 8% acrylamide gel containing a linear gradient (INGENY, Goes, The Netherlands) of 35–60% denaturant (a mixture of urea and formamide). A DGGE ladder, consisting of a mixture of 10 different 16S rRNA gene fragments obtained from *E. coli* clones, was distributed evenly over the gel. After completing electrophoresis (INGENY phorU), the gel was stained with a GelRed-TAE solution (20 μl of GelRed, 100 ml of $1\times$ TAE buffer) for 30 min, and visualized (GeneSnap, Syngene) on an UV-transilluminator (Bio Imaging, Syngene) at an intensity of 400 ms. Community fingerprint images were processed and analyzed with GelCompar II software (Applied Maths, Sint-Martens-Latem, Belgium) and a dendrogram, calculated with the Dice coefficient taking into account the number of shared bands, was constructed from clustering of all data from the gels based on the UPGMA (unweighted pair group method of arithmetic means) algorithm.

Physico-chemical analysis of the biofilm

At the end of the fouling experiment, the fouled membranes were taken out of the bioreactor and the biofilm structure (thickness, composition, density) was investigated by means of (microscopic) fouling measurement techniques: ATR-FTIR, SEM and confocal laser scanning microscopy (CLSM).

ATR-FTIR allows determination of the functional groups of organic membrane foulants. Two coupon replicates were carefully cut out of the fouled membranes, taking care not to disturb or destroy the biofilm. The coupons underwent the same procedure as described earlier.

SEM allows for qualitative description of the morphology of the foulants. Two coupon replicates were carefully cut out of the fouled membranes, taking care not to disturb or destroy the biofilm. The samples were first fixed by immersion in 25 ml of 3% (v v^{-1}) glutaraldehyde solution in 0.1 M phosphate buffer (pH 7.2) for 2 h. The samples were then washed twice for 10 min followed by 1 h in 0.1 M phosphate buffer (pH 7.2). Finally the samples were dehydrated in a seven-step ethanol series in ultrapure H_2O (25, 50, 75, 85, 95, 100, 100%) for 15 min for each dehydration step (Miura et al. 2007; Meng, Zhang, et al. 2007). The dehydrated samples were mounted on a SEM-holder

and were examined at an accelerating voltage of 25 kV and magnifications $250\times$, $1,500\times$ and $10,000\times$.

CLSM is an optical microscope technique which allows for 3-D and depth visualization of biofilm structure as well as determination of biofilm thickness. The biofilm is stained with dyes targeting the biopolymers of interest and the fluorescence light is visualized. Moreover, it may allow for discrimination of the membrane foulants (proteins, bacteria, polysaccharides) and determination of their spatial distribution within the biofilm (Meng et al. 2010). One coupon was carefully cut out of the fouled membranes taking care not to disturb or destroy the biofilm. The coupon was immersed in 25 ml of 0.1 M phosphate buffer and stored in the fridge for 24 h prior to staining and without additional fixation. The biofilm was stained (Lee et al. 2007) and fixed on a microscope cover glass. The images were immediately acquired (Olympus Fluoview Viewer software, version 4.1) with a laser-scanning microscope (FV1000-Ix81, Olympus Fluoview) by means of the objectives UPLanSAPO $40\times/0.90 \infty 0.17/\text{FN}26.5$ (magnification $40\times$) and UPLanSAPO $100\times/1.40\text{oil} \infty 0.17/\text{FN}26.5$ (magnification $100\times$). At magnification $40\times$, depth images were acquired by optical sectioning using steps of $1 \mu\text{m}$, while at magnification $100\times$ the step sizes were set at 0.5 or $0.25 \mu\text{m}$. Biofilm thicknesses were calculated by multiplying the number of slices taken by the size of each step. The image size was adjusted to 512×512 pixels, $1\times$ zoom and an aspect ratio 1:1. Signals were recorded sequentially in the green channel (SYTO 9, excitation at 488 nm, emission at 500–524 nm) and in the red channel (SYTO 62, excitation at 635 nm, emission at 655–755). Finally, the 3-D structure of the biofilm was reconstructed and images were processed (evaluation version, Imaris Bitplane, Zurich, Switzerland).

Results and discussion

The purpose of this study was to elucidate the relation between the specific surface charge (neutral, positive, negative) of PAN membranes and the development and composition of the microbial community in the biofouling layer developed in a long-term run of a submerged laboratory-scale aerobic membrane bioreactor (HT-MBR) operated on protamylasse feed. In the next section (headed MBR operating parameters and characteristics) the performance of the MBR is presented. Four different types of PAN membrane were used, and their performances were determined based on physico-chemical characteristics (*via* ATR-FTIR, SEM, AFM, CA, volume porosity measurement, electrokinetic characterization) and permeability related measurements (CWP, critical flux), as explained in the section headed Membrane characteristics. Finally, membrane biofouling was characterized based

on molecular fingerprinting techniques (PCR-DGGE) and physico-chemical techniques (*via* ATR-FTIR, SEM, CLSM) and discussed in the sections headed Biofouling community characterization and Physico-chemical analysis of the biofilm, respectively.

MBR operating parameters and characteristics

Tables 3 and 4 give an overview of the operating parameters and conditions of the HT-MBR. The HT-MBR was able to remove around 90% of the chemical oxygen demand. The bioreactor exhibited normal biomass concentrations with irregularly shaped flocs and good carbon, nitrogen and

Table 3. Summary of the characteristics and operating parameters of the HT-MBR.

Parameter	Value	Parameter	Value
Reactor volume (l)	37.8	Total cross-flow rate (l day ⁻¹)	25.6 ± 3.1
Activated sludge volume (l)	20	Aeration rate (l min ⁻¹)	10
Protamylase feed solution concentration (ml l ⁻¹)	1.5 → 2.3	Dissolved oxygen concentration (mg O ₂ l ⁻¹)	4.6 ± 0.6
HRT (h)	18.75	SVI (ml g ⁻¹)	153 ± 37
SRT (days)	100	pH	7.81 ± 0.24
TSS (g l ⁻¹)	6.05 ± 1.74	VSS (g l ⁻¹)	5.31 ± 1.79
Average volumetric loading rate (kg COD m ⁻³ day ⁻¹)	1.05	Average sludge loading rate (kg COD kg ⁻¹ MLSS day ⁻¹)	0.17
Temperature (°C)	13.6 ± 1.2		

Values are given as (means ± SD).

HRT: hydraulic retention time; SRT: solid retention time; TSS: total suspended solid; COD: chemical oxygen demand; SVI: sludge volume index; VSS: volatile suspended solid; MLSS: mixed liquor suspended solid.

Table 4. The characteristics of the feed solution, the sludge supernatant and/or the permeate as well as their removal efficiencies (% in the HT-MBR).

Parameter	Feed	Sludge	Permeate	Removal efficiency (%)
COD (mg O ₂ l ⁻¹)	823.1 ± 202.3		71.2 ± 10.2	90.9 ± 2.9
sCOD (mg O ₂ l ⁻¹)		98.2 ± 20.9		
TN (mg TN l ⁻¹)	132.8 ± 39.5		70.7 ± 33.1	49.3 ± 22.9
P (mg PO ₄ -P l ⁻¹)	9.9 ± 3.7		8.4 ± 2.0	25.5 ± 11.8
COD:N:P	100:17:1		100:138:18	

Values are given as (means ± SD).

sCOD: soluble chemical oxygen demand; TN: total nitrogen; P: phosphate.

Table 5. Overview of the membrane types synthesized and used in this work together with their physical properties determined via membrane performance measurements.

Code	Surface roughness (nm) at 1×1 μm scale	Contact angle (°)	Volume porosity (%)	Clean water permeance (l m ⁻² h ⁻¹ bar ⁻¹)	Critical flux at 20°C (l m ⁻² h ⁻¹)	Average fouling rate (mbar day ⁻¹)
PAN (neutral)	6.5 ± 1.6	69.8 ± 1.2	31.5 ± 4.1	1,169.0 ± 310.6	12.0–17.4	0.43
PAN-H (-)	3.8 ± 1.1	18.4 ± 2.1	27.0 ± 3.6	861.6 ± 345.4	17.4–20.9	0.29
PAN-H ^{PAH} (+)	3.2 ± 1.8	52.6 ± 4.1	37.1 ± 4.0	826.7 ± 353.1	12.0–17.4	0.17
PAN-H ^{PAA} (-)	5.3 ± 1.5	8.1 ± 7.2	36.5 ± 7.0	721.9 ± 287.9	7.6–12.0	1.54

phosphate removal efficiencies over the complete experimental period, but the activated sludge settled poorly due to proliferation of filamentous bacteria. This might among other things be due to an unevenly distributed oxygen supply within the bioreactor. Moreover, the sludge was inhabited by a series of non-bacterial microorganisms. Thus, overall the sludge was of good to moderate quality and the membranes seemed to fully retain microorganisms from the sludge suspension.

Membrane characteristics

Table 5 gives an overview of the membranes and their properties. SEM images revealed a typical finger-like macroporous structure with a very thin skin layer from the membrane cross section and quite small pore sizes in the range of 9–21 nm from the membrane surface (Supplementary Figure S1). No apparent difference in surface roughness was observed between membrane types, confirmed by AFM measurements (Supplementary Figures S2 and S3). All membranes exhibited the same high volume porosity of around 30%, indicating that surface modification by hydrolysis and LbL deposition did not significantly alter the membrane structure.

Surface properties analysis

ATR-FTIR spectra revealed the presence of the required functional groups on the membrane surfaces (Supplementary Figure S4). At the pH of the activated sludge suspension (around 7–8), they provided the membranes with neutral properties (C≡N) for the PAN membranes or charged properties (–COO⁻ for PAN-H (-) and PAN-H^{PAA} (-); –NH₃⁺ for PAN-H^{PAH} (+)). The *pKa* value of the polymers PAH and PAA in solution are 8–9 and 5.5–6.5 respectively (Choi and Rubner 2005). Thus, at a pH ~ 7–8 (the pH of the activated sludge suspension), PAA and PAH are nearly fully charged (Ilyas et al. 2016).

The membrane surface properties were analyzed by contact angle measurement and streaming current coefficient, as discussed in more detail in the following paragraph.

CA results confirmed that the PAN (neutral) membrane showed a higher degree of hydrophobicity than the functionalized charged PAN membranes. Compared

to the PAN (neutral) membrane, membrane PAN-H (-) and PAN-H^{PAA} (-) seemed to be more hydrophilic, which was probably due to the large excess of carboxylic groups (Ilyas et al. 2016). On the other hand, compared to membrane PAN-H^{PAA} (-), membrane PAN-H^{PAH} (+) was more hydrophobic. This is due to the PAH terminating layer which is more hydrophobic than the PAA terminating layer, as also found in a previous study (Ilyas et al. 2016).

Figure 1 shows the streaming current coefficient of the membranes. The extensive swelling of the macroporous structures of the membranes does not allow further reliable calculation of the membrane surface zeta potential (Szymczyk et al. 2013). However, some information can still be taken from this measurement.

The charged membranes (PAN-H (-), PAN-H^{PAH} (+) and PAN-H^{PAA} (-)) exhibit a different behavior compared to the PAN (neutral) membrane over the pH range considered. The PAN (neutral) membrane showed a stable negative electrokinetic signal, independent of the pH of the electrolyte solution, and did not have an isoelectric point. All charged membranes exhibited an isoelectric point around pH = 4 and a marked plateau from pH ~5.5, which points to the presence of weak acids. This observation indeed fits for the two negatively charged membranes, PAN-H (-) and PAN-H^{PAA} (-), which had carboxylic groups on their surfaces. For membrane PAN-H^{PAH} (+), the streaming current coefficient values were higher than for membrane PAN-H (-) and PAN-H^{PAA} (-), indicating

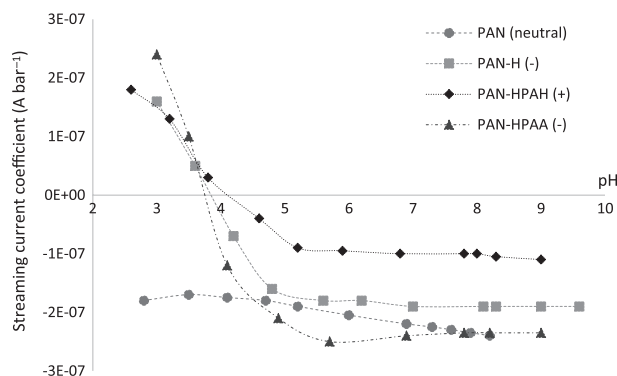


Figure 1. Streaming current coefficient (A bar^{-1}) vs pH for the four membrane types. The intersection of the curves with the x-axis corresponds to the isoelectric point.

less negativity. However, it was expected that membrane PAN-H^{PAH} (+) would show more positive values.

One study of LbL modification with nanofiltration membranes (NF270) shows that a layer of poly(diallyldimethylammonium chloride) (PDADMAC) was able to reverse the zeta potential of the membrane from negative (-25 mV) to positive (+20 mV). When alternated with another layer of polystyrene sulfonate, it switched back to negative (-20 mV) (Malaisamy et al. 2011). However, in the present study, this expected observation was not obtained. This could be due to an inhomogeneous coating of the polyelectrolyte on the membrane surface during the dipcoating step caused by the relatively rough surface of the PAN membranes, which was clearly rougher than NF270 (Hilal et al. 2005; Johnson et al. 2012). Because of this, a substantial contribution by the underlying surface cannot be neglected in this measurement, indicated by the negative values for all membranes (including membrane PAN-H^{PAH} (+), which should be positive). Moreover, due to the high hydrophilicity of the PAN-H membrane (contact angle: 18.4°; see Table 5), a significant part of the experimental streaming current is likely to flow through the underlying porous structure of the PAN-H^{PAH} membrane instead of flowing only over the membrane top surface (Szymczyk et al. 2013). As a result, tangential streaming current measurements performed with the PAN-H^{PAH} membrane may not reflect the actual top surface charge but are likely to include a significant contribution coming from the porous body of the underlying negatively charged PAN-H. On the other hand, it was shown that such a perturbation of electrokinetic measurements by the membrane porous body was negligible in the case of the NF270 membrane (Idil Mouhoumed et al. 2014), probably because there was much less hydrophilic polysulfone sublayer compared with PAN-H considered in the present work.

Permeabilities

Permeability measurements indicated that the membranes were all characterized by a high clean water permeance of around $900 \text{ l m}^{-2} \text{ h}^{-1} \text{ bar}^{-1}$ (Table 5). Thus, together with the observations and conclusions drawn from the physico-chemical measurements, the initial requirement has been fulfilled, namely to obtain neutral and charged

Table 6. Critical flux values at the operating condition of the HT-MBR as well as corrected to a standard temperature of 20°C, for the four membrane types.

Membrane type	Critical flux value at the operation temperature of the HT-MBR ($\text{l m}^{-2} \text{ h}^{-1}$)	Correction of the critical flux value to a standard temperature of 20°C ($\text{l m}^{-2} \text{ h}^{-1}$)
PAN (neutral)	$10.4 < J_c < 15.1$	$12.0 < J_c < 17.4$
PAN-H (-)	$15.1 < J_c < 18.1$	$17.4 < J_c < 20.9$
PAN-H ^{PAH} (+)	$10.4 < J_c < 15.1$	$12.0 < J_c < 17.4$
PAN-H ^{PAA} (-)	$6.6 < J_c < 10.4$	$7.6 < J_c < 12.0$

membranes for which the fouling behavior would be solely determined by charge difference and not by differences in pore size (distribution), clean water permeability or surface roughness.

Table 6 gives the critical flux values of the membrane, as well as the corresponding values corrected to a standard temperature of 20°C. Here the authors have chosen to use a fouling rate threshold value to define the critical flux: J_c is the flux at which the fouling rate exceeds 6 mbar h⁻¹. It can be observed that membranes PAN (neutral) and PAN-H^{PAH} (+) have low J_c values compared to the more hydrophilic PAN-H (-) membrane. The differences in critical flux values may not be attributed to differences in porosity or pore size, but to differences in the degree of hydrophilicity of the membranes. For membrane PAN-H^{PAA} (-), as it is the most hydrophilic membrane, it should exhibit the larger critical flux. However, it is not the case here and this could be due the fact that the added layers on membrane PAN-H^{PAA} (-) has decreased the permeability.

During the fouling experiment, the HT-MBR was operated at a sub-critical level ($\sim 6.5 \text{ l m}^{-2} \text{ h}^{-1}$). Thus, gradual and slow fouling experiments could be conducted without the need to clean the membranes chemically or to apply additional fouling control strategies other than intermittent relaxation.

Biofouling community characterization

Figure 2 represents the dendrogram constructed from the 16S rRNA gene community fingerprint of the membrane biofilms, the activated sludge and the protamylasse feed samples. Although numerous intensive bands are distinguishable, representing the most dominant bacteria in the samples, some weak bands result in a smear unfit for analysis. Most of the sequences exhibited a similarity at the nodes of < 90% (ie < 90% of shared bands). Figure 3 gives the number of operational taxonomic units (OTUs) computed from the fingerprints of the four membrane types at every sample time point. Although it is assumed that each band in the fingerprint corresponds to a different OTU, some bacterial species could have the same G+C DNA content but a different base sequence, thus a single band could represent different species (Boon et al. 2002). Moreover one bacterial species could be represented by different fingerprint G+C sequence micro-heterogeneity and thus produce multiple bands (Boon et al. 2002). Thus, the number of OTUs only gives an approximation of the number and abundance of bacterial species within the community. Moreover, PCR-DGGE is reported to detect only bacterial populations that make up at least 1% of the total community, thus bacterial populations present in very low abundance within the community are mostly

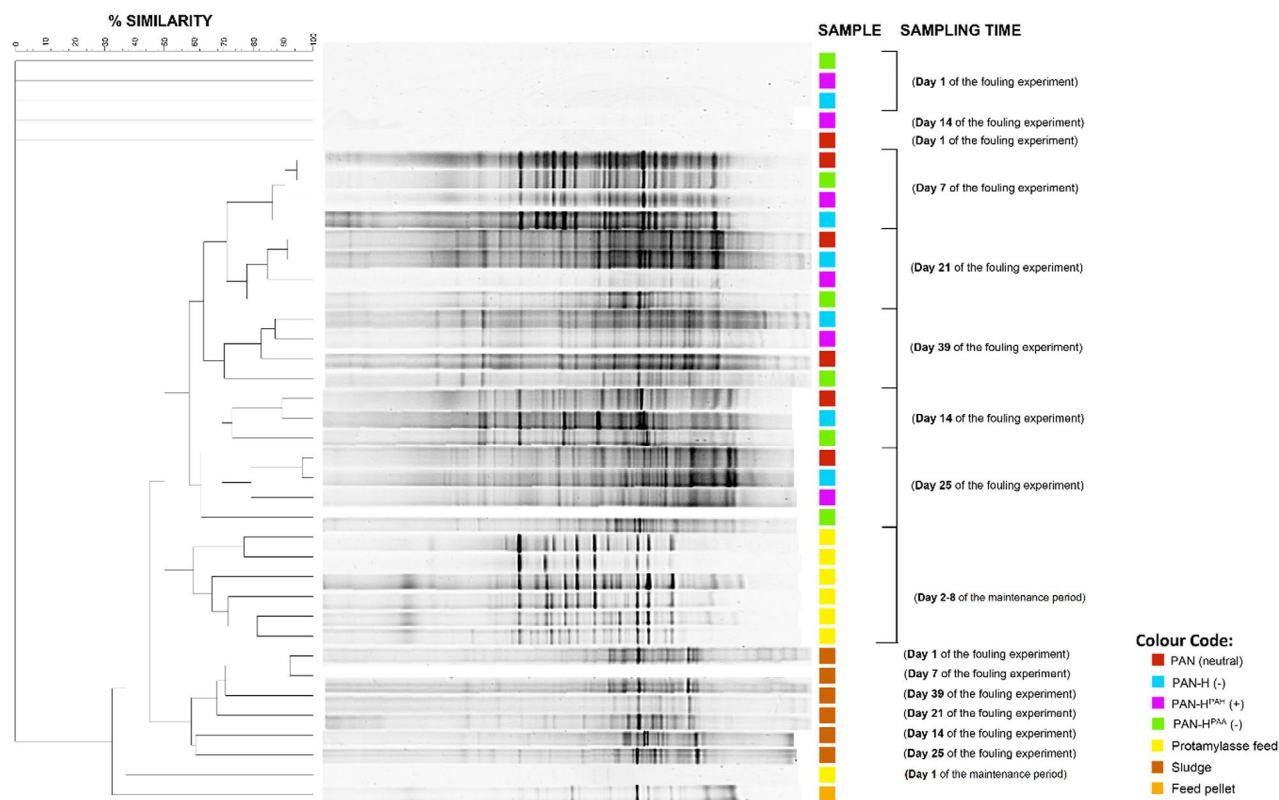


Figure 2. Bacterial 16S rRNA gene community fingerprints (DGGE profile showing differences in community structure and respective dendrogram) derived from membrane biofilms, activated sludge and protamylasse feed solution at different sampling time points. The scale bar represents the percentage similarity at the nodes. The standard markers were removed from the DGGE profile for clarity.

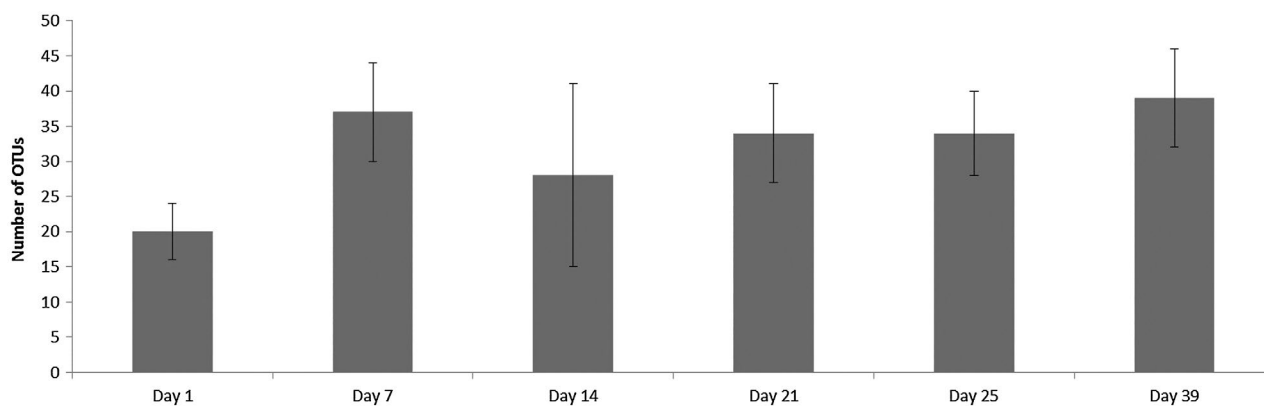


Figure 3. Number of operational taxonomic units derived from the number of bands in the fingerprints of the membrane samples taken at different time points during the fouling experiments. Error bars represent SDs from the mean value based on the band number of the four membrane types ($n = 4$).

excluded from the analysis (Boon et al. 2002; Goodhead et al. 2014).

Based on Figure 2, it may be stated that the planktonic community of activated sludge differs significantly from that of the protamylasse feed, and both differ significantly from the sessile community of the membrane biofilms, independently of the sampling time point or on the membrane type. Among other publications (Zhang, Choi, et al. 2006; Jinhua et al. 2006), Huang et al. (2008) and Piasecka et al. (2012) observed that most of the OTUs detected in planktonic biomass were not detected in the biofilm fingerprints (Huang et al. 2008; Piasecka et al. 2012), or at least not in the same relative abundance (Miura et al. 2007). While the α -, β -, γ - and δ -Proteobacteria are the dominant species found in biofilms, the activated sludge communities of both aerobic and anaerobic MBRs were reported to be dominated by α -, β - or γ -Proteobacteria (Wagner et al. 1994; Boon et al. 2002; Piasecka et al. 2012) (eg *Pseudomonas* sp. which is reported to always be present in activated sludge (Khan et al. 2013; Waheed et al. 2013)), Bacteroidetes (Wan et al. 2011; Piasecka et al. 2012) and Gram-positive bacteria characterized by a high G+C DNA content (generally > 50%) (Wagner et al. 1994). The latter include the class Actinobacteria and more specifically the filamentous actinomycetes (Boon et al. 2002; Ventura et al. 2007), to which *M. parvicella*, a filamentous bacterium predominant in sludge belongs (McIlroy et al. 2013). Most of these abundant planktonic bacteria have not been observed to colonize membrane surfaces, which may explain the differences in the planktonic and membrane-associated communities in the present experiments.

The sludge profiles exhibit fluctuations over time during the fouling experiment (eg variation in relative abundance of common bands), the protamylasse feed profiles do not change over time during the experiments (data of days 2–8 of the maintenance period). It has already been reported that the function and structure of the planktonic

community in the sludge suspension are highly diverse but do fluctuate over time with changes in the condition of the HT-MBR (Huang et al. 2008; Piasecka et al. 2012). As seen from Figure 2, the protamylasse feed sample of day 1 of the maintenance period differs significantly from the feed samples of the other days of the maintenance period, showing it did not contain enough biomass as already indicated by microscopic investigation. In addition, the feed pellet developing at the bottom of the feed tank exhibited a lower microbial diversity than the feed samples taken from the solution.

Due to low biomass on the initial day of fouling, it is not clear whether there is a marked difference in microbial communities on the different membranes. Membrane PAN (neutral) could have exhibited a lower fouling degree and biofilm diversity than PAN-H^{PAH} (+) (Pasmore et al. 2001), and itself could have had a lower fouling tendency than the PAN-H (-) and PAN-H^{PAH} (-) membranes (Gottenbos et al. 2001), due to the influence of the surface charge. However, the surface effect would eventually fade out as the initial stages of fouling are surpassed due to deposition and accumulation of material which covers the membrane surface.

Finally, the results reveal that the bacterial communities developing on the membranes differ between sampling time points but not between membrane types. This suggests that the relative abundance and structure of the bacterial population changes with time due to interactions between members of the biofilm as well as with the external environment (eg fluctuating operating conditions and hydrodynamics). These interactions modify the local biofilm environment with time by creating ecological protective niches within the biofilm based on physical gradients, leading to exclusion or favoring of existing members within the community (Martiny et al. 2003). β -Proteobacteria, or more specifically *Rhodocyclus*- or *Ralstonia*-related bacteria, were reported to be the dominant phylogenetic group

in mature biofilms, although the relative dominance of the α -, β -, γ - and δ -Proteobacteria in biofilms may vary with time due to, for example, variations in the mixed liquor viscosity or aeration rate (Miura et al. 2007). For instance, it has been reported that nutrient-rich environments favor the γ -Proteobacteria against the β -subgroup (Miura et al. 2007). Martiny et al. (2003), who examined the development of biofilms in a drinking water system over three years, found that the biofilm communities stabilized only after two years of operation (Martiny et al. 2003). However, the fingerprints did not indicate an increase in bacterial species since no significant increase in OTUs was observed throughout the sample time points (Student's t , $0.10 < p < 0.80$) (Figure 3). Moreover, the observation suggests that although there might be a selective attachment of bacteria during the initial stages of fouling, the local characteristics of the membrane (here: charge) do not play a decisive role in the long term in selecting key foulants.

Physico-chemical analysis of the biofilm

Figure 4 shows ATR-FTIR spectra of the fouled membranes. When comparing to the pristine spectra (Supplementary Figure S1), the only two peaks that are still visible are the ($-\text{CH}-$) bend and stretch vibrations, at wavenumbers $1,450\text{ cm}^{-1}$ and $2,930\text{ cm}^{-1}$ respectively (Meng, Zhang, et al. 2007; Bilad et al. 2011b), which could be attributed to the PAN backbone as well as to the carbon backbone of the biopolymers. The nitrile ($\text{C}\equiv\text{N}$) functional group of the membrane material cannot be discerned any longer, suggesting that the biofilm did cover the membrane surface well.

Proteins can be discerned from the peaks around $1,530$ and $1,630\text{ cm}^{-1}$ which are specific for the secondary conformation of proteins, called amide II (N-H bend and C-N stretch) and amide I ($\text{C}=\text{O}$ stretch) respectively (Meng, Shi, et al. 2007; Bilad et al. 2011b). The peak at $1,630\text{ cm}^{-1}$ could also be attributed to aromatic compounds or humic-like substances (Meng et al. 2010). Additionally, the peak around $1,400\text{ cm}^{-1}$ corresponds to the asymmetric stretch of carboxyl ($-\text{COO}-$) or carbonyl ($\text{C}=\text{O}$) groups of amino acids (Meng et al. 2010). The hydroxyl (O-H) stretch is represented by the broad peak at $3,270\text{ cm}^{-1}$ (Meng, Zhang, et al. 2007). The peak around $1,035\text{ cm}^{-1}$ may represent (C-O) stretch vibration of polysaccharides or polysaccharide-like substances (Meng, Zhang, et al. 2007). Finally the peak around $1,230\text{ cm}^{-1}$ can be assigned to the phosphate vibrations in nucleotides (Landa et al. 1997).

All functional groups distinguished here suggest the presence of bacteria, protein and polysaccharide-like substances (biopolymers, humic substances) in the cake layer, mostly originating directly from deposition of activated sludge material (Bilad et al. 2011b).

Figure 5 shows the rough structure of the biofilm that develops on the surface of the 13% PAN (neutral) membrane after 40 days of fouling. Comparison between fouled membranes (Figure 5B) and clean/pristine membranes (Supplementary Figure S2) indicates that the biofilm and deposited particles cover the membrane surface well since the surface features of the pristine membrane cannot be discerned. Moreover, the images show a clear size difference between the components of the biofilm (μm range) and the depressions and pores (nm range) of the pristine membrane, illustrating why the membranes were capable

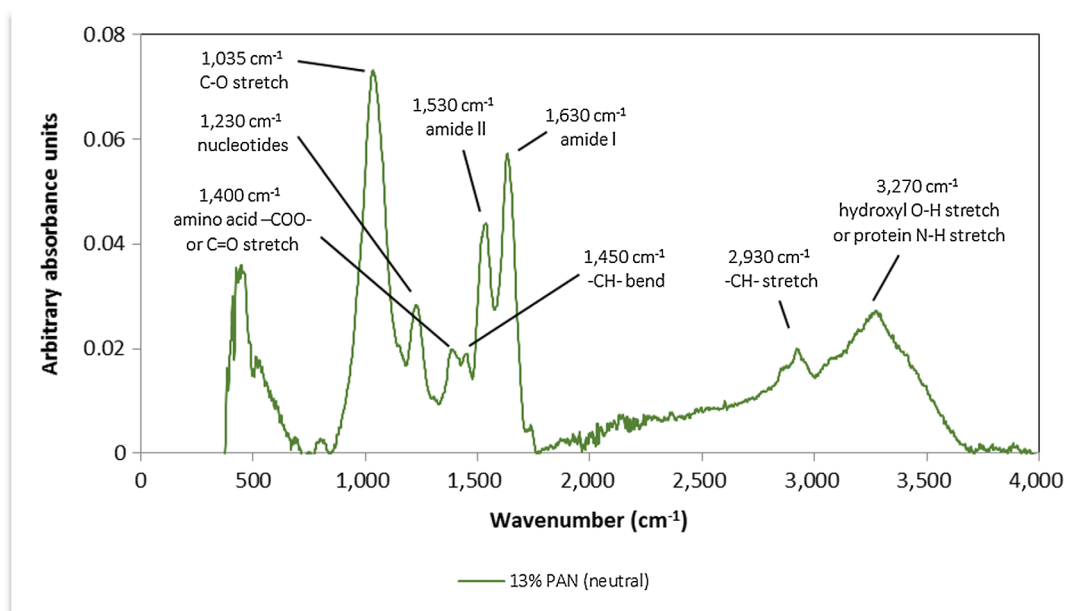


Figure 4. ATR-FTIR graph of the fouling layer of membrane 13% PAN (neutral).

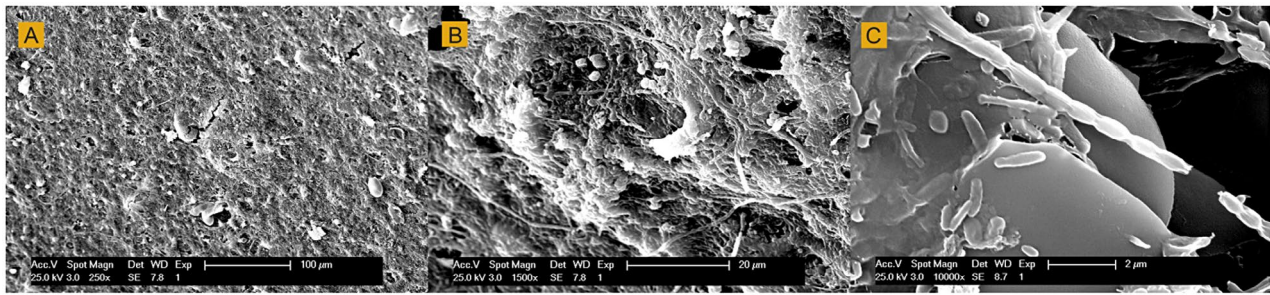


Figure 5. SEM surface images of the fouling layer of membrane 13% PAN (neutral) at different magnifications.

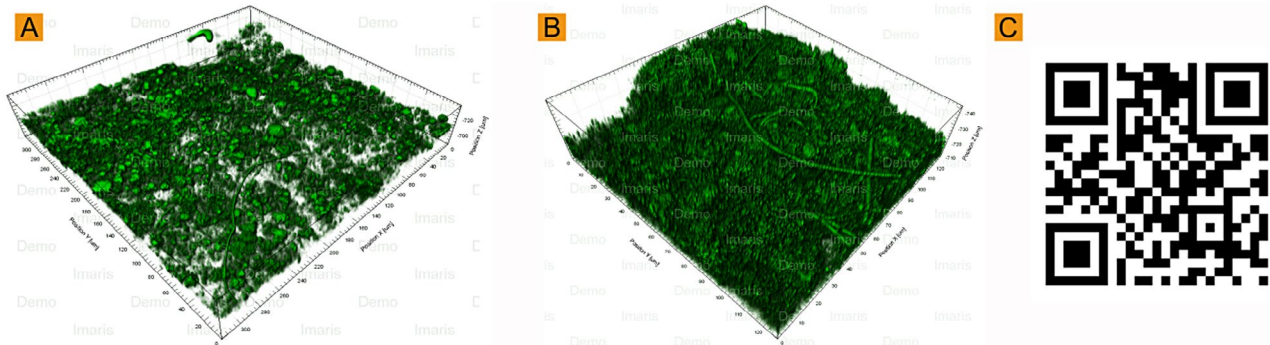


Figure 6. CLSM images of the biofouling layer of membrane 13% PAN (neutral) at magnifications 40 \times and 320 \times 320 μm surface area (A) and magnification 100 \times and 125 \times 125 μm surface area (B). The QR code (C) gives access to a Youtube video highlighting the 3-D structure of the biofilm (100 \times) by migration of the fluorescence signal over the cake depth. The images and the video were processed by means of the software evaluation version of Imaris Bitplane. <http://youtu.be/96bUH84PlmM>.

of retaining particulate matter and bacterial species from the sludge suspension and the biofilm. A number of spherical and rod-shaped bioparticles (eg *Bacillus* sp.) as well as a network of filaments could be distinguished, embedded in a matrix of what it is assumed to be biopolymers or an artifact of SEM preparation (see for instance the gel-like structure surrounding the chains of rods in Figure 5C). Although SEM gives information on the biofilm structure and allows for discrimination based on size and shape of the particles, it gives only limited information on the nature of the foulants (organic, inorganic) or on the specific bacterial species. Moreover, the rather stringent SEM pretreatment may alter the original structure of the fouling layer (Meng et al. 2010).

Figure 6 represents the 3-D architecture of the biofilm which developed on the membrane surface of 13% PAN (neutral) after operation for 40 days and at different magnifications. It also gives access to a video highlighting the 3-D composition of the fouling layer by migration of the fluorescence signal over the cake depth. The images are represented in green, since staining and visualization with SYTO 62 failed.

The biofilm was $\sim 45 \mu\text{m}$ in height. It has been reported that biofilm thickness does not depend on the operating conditions of the MBR, but tends to converge to the same order of magnitude, influenced by the balance between

nutrient level, shear forces and transmembrane pressure (Ivniisky et al. 2007; Huang et al. 2008). The biofilm was dense and mainly composed of discrete clusters of apparently a few dominant bacteria at different locations and at different heights spread across the membrane surface, as can be seen in the video (QR code in Figure 6). The apparent low diversity may be in contradiction with the fingerprinting results, which suggested a highly diverse biofilm. Since the samples were not fixated prior to the CLSM analysis, a considerable amount of biofilm material may have been lost. However, the discrete bacterial clusters may be characteristic to biofilms in development, since mature biofilms have been reported to consist of an even and smooth community structure without patches composed of independent populations (Martiny et al. 2003). This thus suggests that each cluster or colony developed from one bacterium initially attaching to the membrane surface or that bacteria seek each other and preferably assemble rather than living as single individuals elsewhere in the biofilm.

Conclusions

The development and composition of the microbial community in the biofouling layer were investigated over a period of 40 days in a submerged laboratory-scale aerobic

membrane bioreactor (HT-MBR) using PAN-based membranes with different surface charge. PCR-DGGE fingerprinting revealed that the planktonic communities of the activated sludge exhibited differentiated branching in the dendrogram from the sessile communities of the biofilm, independently of the sampling time point or on the membrane type. Bacterial populations from the sludge suspension were thus selectively enriched within the biofilms. Variations in biofilm community structure and composition were monitored over time, suggesting that local variations in the biofilm and the gradual development of ecological protective niches favor or exclude specific bacterial populations. The largest time-dependent difference in number of OTUs was observed between the samples from the first sampling time point and the samples taken at the other time points, probably explained by a lack of bacterial product suitable for analysis. Finally, the bacterial communities did not differ between membrane types, suggesting that the membrane surface charges do not affect biofilm community composition. Thus, membrane charge did not play a decisive role in the long-term selection of the key foulants.

Acknowledgements

The authors acknowledge Alexander Volodine (Department of Physics and Astronomy, KU Leuven) for AFM measurements, Lynn Lemoine and Benjamin Horemans (Division of Soil and Water Management, KU Leuven) for helping with the DGGE and CLSM measurement, Prof. Ilse Smets (Department of Chemical Engineering, KU Leuven) for her advice concerning the activated sludge and ProCESS Lab (Process Engineering for Sustainable System, KU Leuven) for the usage of a contact angle measurement instrument.

Disclosure statement

No potential conflict of interest was reported by the authors.

Funding

KU Leuven provided financial support in the frame of the FWO [grant number G.0808.10 N], [grant number G.A.043.12 N]; ERA-Net New INDIGO, OT [11/061], IOF-KP [IOFKP/13/004]; the Belgian Federal Government provided an IAP grant.

References

- Bilal MR, Declerck P, Piasecka A, Vanysacker L, Yan X, Vankelecom IFJ. 2011a. Development and validation of a high-throughput membrane bioreactor (HT-MBR). *J Membr Sci.* 379:146–153. doi:10.1016/j.memsci.2011.05.052.
- Bilal MR, Declerck P, Piasecka A, Vanysacker L, Yan X, Vankelecom IFJ. 2011b. Treatment of molasses wastewater in a membrane bioreactor: influence of membrane pore size. *Sep Purif Technol.* 78:105–112.
- Boon N, De Windt W, Verstraete W, Top EM. 2002. Evaluation of nested PCR-DGGE (denaturing gradient gel electrophoresis) with group-specific 16S rRNA primers for the analysis of bacterial communities from different wastewater treatment plants. *FEMS Microbiol Ecol.* 39:101–112.
- Choi J, Rubner MF. 2005. Influence of the degree of ionization on weak polyelectrolyte multilayer assembly. *Macromolecules.* 38:116–124. doi:10.1021/ma048596o.
- Fan F, Zhou H, Husain H. 2006. Identification of wastewater sludge characteristics to predict critical flux for membrane bioreactor processes. *Water Res.* 40:205–212. doi:10.1016/j.watres.2005.10.037.
- Field RW, Wu D, Howell JA, Gupta BB. 1995. Critical flux concept for microfiltration fouling. *J Membr Sci.* 100:259–272. doi:10.1016/0376-7388(94)00265-Z.
- Goodhead AK, Head IM, Snape JR, Davenport RJ. 2014. Standard inocula preparations reduce the bacterial diversity and reliability of regulatory biodegradation tests. *Environ Sci Pollut Res.* 21:9511–9521. doi:10.1007/s11356-013-2064-4.
- Gottenbos B, Grijpma DW, van der Mei HC, Feijen J, Busscher HJ. 2001. Antimicrobial effects of positively charged surfaces on adhering gram-positive and gram-negative bacteria. *J Antimicrob Chemother.* 48:7–13. doi:10.1093/jac/48.1.7.
- Hilal N, Al-Zoubi H, Darwish NA, Mohammad AW. 2005. Characterisation of nanofiltration membranes using atomic force microscopy. *Desalination.* 177:187–199. doi:10.1016/j.desal.2004.12.008.
- Hołda AK, Vankelecom IFJ. 2015. Understanding and guiding the phase inversion process for synthesis of solvent resistant nanofiltration membranes. *J Appl Polym Sci.* 132:42130.
- Huang L-N, De Wever H, Diels L. 2008. Diverse and distinct bacterial communities induced biofilm fouling in membrane bioreactors operated under different conditions. *Environ Sci Technol.* 42:8360–8366. doi:10.1021/es801283q.
- Idil Mouhoumed E, Szymczyk A, Schäfer A, Paugam L, La YH. 2014. Physico-chemical characterization of polyamide NF/RO membranes: insight from streaming current measurements. *J Membr Sci.* 461:130–138. doi:10.1016/j.memsci.2014.03.025.
- Ilyas S, Joseph N, Szymczyk A, Volodin A, Nijmeijer K, de Vos WM, Vankelecom IFJ. 2016. Weak polyelectrolyte multilayers as tunable membranes for solvent resistant nanofiltration. *J Membr Sci.* 514:322–331. doi:10.1016/j.memsci.2016.04.073.
- Ivniitsky H, Katz I, Minz D, Volvovic G, Shimoni E, Kesselman E, Semiat R, Dosoretz CG. 2007. Bacterial community composition and structure of biofilms developing on nanofiltration membranes applied to wastewater treatment. *Water Res.* 41:3924–3935. doi:10.1016/j.watres.2007.05.021.
- Jinhua P, Fukushi K, Yamamoto K. 2006. Bacterial community structure on membrane surface and characteristics of strains isolated from membrane surface in submerged membrane bioreactor. *Sep Sci Technol.* 41:1527–1549. doi:10.1080/01496390600683571.
- Johnson DJ, Al Malek SA, Al-Rashdi BAM, Hilal N. 2012. Atomic force microscopy of nanofiltration membranes: effect of imaging mode and environment. *J Membr Sci.* 389:486–498. doi:10.1016/j.memsci.2011.11.023.
- Joseph N, Ahmadiannamini P, Hooogenboom R, Vankelecom IFJ. 2014. Layer-by-layer preparation of polyelectrolyte

- multilayer membranes for separation. *Polym Chem.* 5:1817–1831. doi:10.1039/C3PY01262 J.
- Jucker BA, Harms H, Zehnder AJB. 1996. Adhesion of the positively charged bacterium *Stenotrophomonas (Xanthomonas) maltophilia* 70401 to glass and teflon. *J Bacteriol.* 178:5472–5479. doi:10.1128/jb.178.18.5472-5479.1996.
- Khan SJ, Parveen F, Ahmad A, Hashmi I, Hankins N. 2013. Performance evaluation and bacterial characterization of membrane bioreactors. *Bioresour Technol.* 141:2–7. doi:10.1016/j.biortech.2013.01.140.
- Kochkodan V, Hilal N. 2015. A comprehensive review on surface modified polymer membranes for biofouling mitigation. *Desalination.* 356:187–207. doi:10.1016/j.desal.2014.09.015.
- Landa AS, Van Der Mei HC, Busscher HJ. 1997. Detachment of linking film bacteria from enamel surfaces by oral rinses and penetration of sodium lauryl sulphate through an artificial oral biofilm. *Adv Dent Res.* 11:528–538. doi:10.1177/08959374970110042201.
- Larsen MH, Biermann K, Tandberg S, Hsu T, Jacobs WR. 2007. Genetic manipulation of *Mycobacterium tuberculosis*. *Curr Protoc Microbiol.* Chapter 10: Unit 10A.2.
- Le Clech P, Jefferson B, Chang IS, Judd SJ. 2003. Critical flux determination by the flux-step method in a submerged membrane bioreactor. *J Membr Sci.* 227:81–93. doi:10.1016/j.memsci.2003.07.021.
- Le-Clech P. 2010. Membrane bioreactors and their uses in wastewater treatments. *Appl Microbiol Biotechnol.* 88:1253–1260. doi:10.1007/s00253-010-2885-8.
- Le-Clech P, Chen V, Fane TAG. 2006. Fouling in membrane bioreactors used in wastewater treatment. *J Membr Sci.* 284:17–53. doi:10.1016/j.memsci.2006.08.019.
- Lee W-N, Chang I-S, Hwang B-K, Park P-K, Lee C-H, Huang X. 2007. Changes in biofilm architecture with addition of membrane fouling reducer in a membrane bioreactor. *Process Biochem.* 42:655–661. doi:10.1016/j.procbio.2006.12.003.
- Li X, Feyter S De, Chen D, Aldea S, Vandezande P, Prez FDu, Vankelecom IFJ. 2008. Solvent-resistant nanofiltration membranes based on multilayered polyelectrolyte complexes. *Chem Mater.* 20:3876–3883. doi:10.1021/cm703072 k.
- Liu CX, Zhang DR, He Y, Zhao XS, Bai R. 2010. Modification of membrane surface for anti-biofouling performance: effect of anti-adhesion and anti-bacteria approaches. *J Membr Sci.* 346:121–130. doi:10.1016/j.memsci.2009.09.028.
- Malaisamy R, Talla-Nwafo A, Jones KL. 2011. Polyelectrolyte modification of nanofiltration membrane for selective removal of monovalent anions. *Sep Purif Technol.* 77:367–374. doi:10.1016/j.seppur.2011.01.005.
- Mansouri J, Harrisson S, Chen V. 2010. Strategies for controlling biofouling in membrane filtration systems: challenges and opportunities. *J Mater Chem.* 20:4567. doi:10.1039/b926440j.
- Marbelia L, Bilad MR, Piasecka A, Jishna PS, Naik PV, Vankelecom IFJ. 2016. Study of PVDF asymmetric membranes in a high-throughput membrane bioreactor (HT-MBR): influence of phase inversion parameters and filtration performance. *Sep Purif Technol.* 162:6–13. doi:10.1016/j.seppur.2016.02.008.
- van der Marel P, Zwijnenburg A, Kemperman A, Wessling M, Temmink H, van der Meer W. 2009. An improved flux-step method to determine the critical flux and the critical flux for irreversibility in a membrane bioreactor. *J Membr Sci.* 332:24–29. doi:10.1016/j.memsci.2009.01.046.
- Martiny AC, Jørgensen TM, Albrechtsen H-J, Arvin E, Molin S. 2003. Long-term succession of structure and diversity of a biofilm formed in a model drinking water distribution system. *Appl Environ Microbiol.* 69:6899–6907. doi:10.1128/AEM.69.11.6899-6907.2003.
- McIlroy SJ, Kristiansen R, Albertsen M, Karst SM, Rossetti S, Nielsen JL, Tandoi V, Seviour RJ, Nielsen PH. 2013. Metabolic model for the filamentous “*Candidatus Microthrix parvicella*” based on genomic and metagenomic analyses. *ISME J.* 7:1161–1172. doi:10.1038/ismej.2013.6.
- Meng F, Chae S-R, Drews A, Kraume M, Shin H-S, Yang F. 2009. Recent advances in membrane bioreactors (MBRs): membrane fouling and membrane material. *Water Res.* 43:1489–1512. doi:10.1016/j.watres.2008.12.044.
- Meng F, Shi B, Yang F, Zhang H. 2007. Effect of hydraulic retention time on membrane fouling and biomass characteristics in submerged membrane bioreactors. *Bioprocess Biosyst Eng.* 30:359–367. doi:10.1007/s00449-007-0132-1.
- Meng F, Zhang H, Yang F, Liu L. 2007. Characterization of cake layer in submerged membrane bioreactor. *Environ Sci Technol.* 41:4065–4070. doi:10.1021/es062208b.
- Meng F, Liao B, Liang S, Yang F, Zhang H, Song L. 2010. Morphological visualization, componential characterization and microbiological identification of membrane fouling in membrane bioreactors (MBRs). *J Membr Sci.* 361:1–14. doi:10.1016/j.memsci.2010.06.006.
- Miura Y, Watanabe Y, Okabe S. 2007. Membrane biofouling in pilot-scale membrane bioreactors (MBRs) treating municipal wastewater: impact of biofilm formation. *Environ Sci Technol.* 41:632–638. doi:10.1021/es0615371.
- Pasmore M, Todd P, Smith S, Baker D, Silverstein J, Coons D, Bowman CN. 2001. Effects of ultrafiltration membrane surface properties on *Pseudomonas aeruginosa* biofilm initiation for the purpose of reducing biofouling. *J Membr Sci.* 194:15–32. doi:10.1016/S0376-7388(01)00468-9.
- Piasecka A, Souffreau C, Vandepitte K, Vanysacker L, Bilad RM, De Bie T, Hellemans B, De Meester L, Yan X, Declerck P, Vankelecom IFJ. 2012. Analysis of the microbial community structure in a membrane bioreactor during initial stages of filtration. *Biofouling.* 28:225–238. doi:10.1080/08927014.2012.662640.
- Roosjen A, Norde W, van der Mei HC, Busscher HJ. 2006. The use of positively charged or low surface free energy coatings versus polymer brushes in controlling biofilm formation. *Prog Colloid Polym Sci.* 132:138–144. doi:10.1007/b104970.
- Schaepe J, Vandecasteele C. 2001. Evaluating the charge of nanofiltration membranes. *J Membr Sci.* 188:129–136. doi:10.1016/S0376-7388(01)00368-4.
- Stoodley P, Sauer K, Davies DG, Costerton JW. 2002. Biofilms as complex differentiated communities. *Annu Rev Microbiol.* 56:187–209. doi:10.1146/annurev.micro.56.012302.160705.
- Szymczyk A, Dirir YI, Picot M, Nicolas I, Barrière F. 2013. Advanced electrokinetic characterization of composite porous membranes. *J Membr Sci.* 429:44–51. doi:10.1016/j.memsci.2012.11.076.

- Vandezande P, Li X, Gevers LEM, Vankelecom IFJ. 2009. High throughput study of phase inversion parameters for polyimide-based SRNF membranes. *J Membr Sci.* 330:307–318. doi:10.1016/j.memsci.2008.12.068.
- Vanysacker L, Boerjan B, Declerck P, Vankelecom IFJ. 2014. Biofouling ecology as a means to better understand membrane biofouling. *Appl Microbiol Biotechnol.* 98:8047–8072. doi:10.1007/s00253-014-5921-2.
- Ventura M, Canchaya C, Tauch A, Chandra G, Fitzgerald GF, Chater KF, van Sinderen D. 2007. Genomics of Actinobacteria: tracing the evolutionary history of an ancient phylum. *Microbiol Mol Biol Rev.* 71:495–548. doi:10.1128/MMBR.00005-07.
- Wagner M, Erhart R, Manz W, Amann R, Lemmer H, Wedi D, Schleifer K. 1994. Development of an rRNA-targeted oligonucleotide probe specific for the genus *Acinetobacter* and its application for *in situ* monitoring in activated sludge. *Appl Environ Microbiol.* 60:792–800.
- Waheed H, Hashmi I, Naveed AK, Khan SJ. 2013. Molecular detection of microbial community in a nitrifying–denitrifying activated sludge system. *Int Biodeterior Biodegradation.* 85:527–532. doi:10.1016/j.ibiod.2013.05.009.
- Wan C-Y, De Wever H, Diels L, Thoeye C, Liang J-B, Huang L-N. 2011. Biodiversity and population dynamics of microorganisms in a full-scale membrane bioreactor for municipal wastewater treatment. *Water Res.* 45:1129–1138. doi:10.1016/j.watres.2010.11.008.
- Ye Y, Le-Clech P, Chen V, Fane AG. 2005. Evolution of fouling during crossflow filtration of model EPS solutions. *J Membr Sci.* 264:190–199. doi:10.1016/j.memsci.2005.04.040.
- Zhang J, Chua HC, Zhou J, Fane AG. 2006. Factors affecting the membrane performance in submerged membrane bioreactors. *J Membr Sci.* 284:54–66. doi:10.1016/j.memsci.2006.06.022.
- Zhang K, Choi H, Dionysiou DD, Sorial GA, Oerther DB. 2006. Identifying pioneer bacterial species responsible for biofouling membrane bioreactors. *Environ Microbiol.* 8:433–440. doi:10.1111/emi.2006.8.issue-3.